Characteristics of the phase transition near 147 K in $Sr_3Ir_4Sn_{13}$

C. N. Kuo,[1] H. F. Liu,[1] C. S. Lue,[1,2,*] L. M. Wang,[3,†] C. C. Chen,[4] and Y. K. Kuo[4,‡]

[1]*Department of Physics, National Cheng Kung University, Tainan 70101, Taiwan*

[2]*Taiwan Consortium of Emergent Crystalline Materials, Ministry of Science and Technology, Taipei 10601, Taiwan*

[3]*Department of Physics, National Taiwan University, Taipei 10601, Taiwan*

[4]*Department of Physics, National Dong Hwa University, Hualien 97401, Taiwan*

In order to assess the phase transition nature in $Sr_3Ir_4Sn_{13}$, we have carried out the electrical resistivity, Hall coefficient, Seebeck coefficient, thermal conductivity, specific heat, and ^{119}Sn nuclear magnetic resonance (NMR) measurements, mainly focusing on the signatures around the phase transition temperature $T^* = 147$ K. The phase transition has been characterized by marked features near T^* in all measured physical quantities. In particular, the Hall measurement reveals the abrupt change in both magnitude and sign of the charge carriers below T^*, providing strong evidence for the Fermi surface reconstruction associated with this phase transition. Moreover, the NMR observations indicate the presence of the splitting of the resonance lines below T^* which could be accounted for by the local distortion of the Sn2 icosahedra within the $Pm\bar{3}n$ phase. The NMR Knight shift analysis further provides microscopic evidence for the reduction in both Sn $5s$ and Ir $5d$ electronic states near the Fermi surfaces of $Sr_3Ir_4Sn_{13}$. With respect to these observations, it suggests that the strong interplay between electronic and structural instability is responsible for the peculiar phase transition in $Sr_3Ir_4Sn_{13}$.

I. INTRODUCTION

$Sr_3Ir_4Sn_{13}$ has been found to be a superconductor with a superconducting transition temperature T_c of about 5 K, and its superconductivity has been characterized by a strong-coupling BCS scenario with an isotropic s-wave paring symmetry [1]. This material has been of current interest due to indications of a possible charge-density-wave (CDW) phase transition at $T^* = 147$ K. The CDW-like features manifest themselves by a distinct hump in the electrical resistivity and a sudden drop in the magnetic susceptibility near T^* [2]. Moreover, Klintberg and coworkers noted weak superlattice reflections in the single-crystal x-ray diffraction (XRD) data of $Sr_3Ir_4Sn_{13}$ below T^* [2]. Such an observation has been associated with the structural distortion from a simple cubic to a body-centered cubic superstructure with almost doubling of the lattice parameter, presumably related to the formation of the CDW [2].

The titled compound of $Sr_3Ir_4Sn_{13}$ crystallizes in a three-dimensional (3D) $Yb_3Rh_4Sn_{13}$-type structure (space group $Pm\bar{3}n$) at room temperature [1,2]. While there is general agreement that the CDW in 3D crystal structures arises from the modulation wave vectors along particular directions driven by Fermi-surface nesting, CDW transitions in 3D systems are not ubiquitous. Several ternary rare-earth transition-metal silicides ($R_5M_4Si_{10}$) and nickel-based carbides ($RNiC_2$) have been classified as the 3D CDW members [3–18]. Among these compounds, $Lu_5Ir_4Si_{10}$ is a well-studied prototype [3–10]. Pronounced anomalies observed in the thermal and electrical transport measurements of $Lu_5Ir_4Si_{10}$ have been realized by the Fermi-surface reconstruction along with the CDW ordering [3–9]. With this respect, the examination of the change of electronic features, especially focusing on the temperature region in the vicinity of T^*, would be essential to elucidate the intriguing phase transition in $Sr_3Ir_4Sn_{13}$.

In this work, we performed a detailed study of single-crystalline $Sr_3Ir_4Sn_{13}$ by means of the electrical resistivity (ρ), Hall coefficient (R_H), Seebeck coefficient (S), thermal conductivity (κ), specific heat (C_P), as well as ^{119}Sn nuclear magnetic resonance (NMR) measurements to shed light on the nature of the phase transition. Anomalous features near $T^* = 147$ K have been discerned in the temperature dependencies of these measured physical quantities. The NMR characteristics are in good agreement with the lattice distortion scenario and further provide microscopic evidence for the reduction in both Ir $5d$ and Sn $5s$ electronic states below T^*. Remarkably, the observed phase transition behavior in $Sr_3Ir_4Sn_{13}$ bear a striking resemblance to a CDW ordering in many aspects.

II. RESULTS AND DISCUSSION

Single crystals of $Sr_3Ir_4Sn_{13}$ were grown by the Sn self-flux method. High-purity elements were mixed in the molar ratio of Sr:Ir:Sn = 2.5:1:25 and sealed in an evacuated quartz tube. The tube was heated up to 1323 K and then cooled to 773 K over 72 h. The excessive Sn flux was etched in diluted hydrochloric acid. The obtained crystals have dimensions of several millimeters. A room-temperature XRD measurement taken with Cu K_α radiation on the powdered single-crystal specimen was identified within the expected $Pm\bar{3}n$ phase. The lattice constant $a = 9.7964$ Å was determined for our $Sr_3Ir_4Sn_{13}$ sample, close to the previously reported value [2]. For the transport measurements, the electrical current flows along the direction perpendicular to the (110) plane of the crystal, which has been confirmed by the XRD with the result shown in the lower inset of Fig. 1.

---

*cslue@mail.ncku.edu.tw
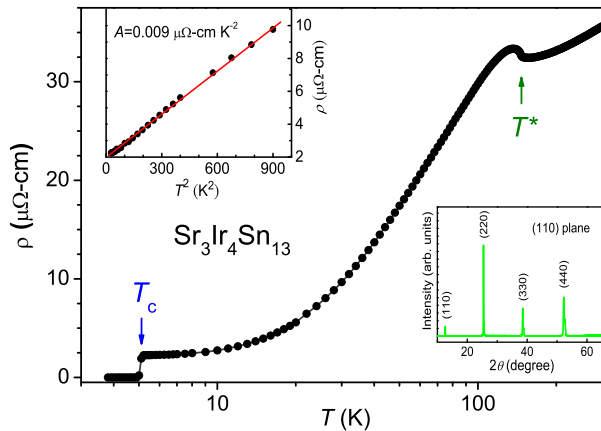
†liminwang@ntu.edu.tw

‡ykkuo@mail.ndhu.edu.tw

FIG. 1. (Color online) Electrical resistivity ρ as a function of temperature for $Sr_3Ir_4Sn_{13}$. The upper inset displays a plot of ρ vs T^2, showing a linear relation between 5 and 30 K. The lower inset gives a room-temperature single-crystal x-ray diffraction pattern from the (110) plane of $Sr_3Ir_4Sn_{13}$. Reflections are indexed with respect to the $Yb_3Rh_4Sn_{13}$-type structure (space group $Pm\bar{3}n$).

A. Electrical resistivity

Data of the electrical resistivity ρ were obtained using a standard four-point probe method. The observed electrical resistivity for $Sr_3Ir_4Sn_{13}$ is displayed in Fig. 1. The temperature dependence of ρ is very similar to that reported by Klintberg *et al.* [2], showing a distinct hump near $T^* = 147$ K and a superconducting phase transition below $T_c = 5$ K. The normal state resistivity between 5 and 30 K can be described well to a power law,

$$\rho(T) = \rho_o + AT^2, \tag{1}$$

where ρ_o is the residual resistivity and A is the temperature coefficient of the electric resistivity. In the upper inset of Fig. 1, we showed the plot of ρ vs T^2, with the linear relation yielding $\rho_o = 1.93$ $\mu\Omega$ cm and $A = 0.009$ $\mu\Omega$ cm/K^2. The residual resistivity ρ_o may arise from the scattering due to domain boundaries and/or defects by electrons. The small value of ρ_o indicates the high quality of the present single crystal and gives an estimate of the residual resistivity ratio [RRR, $\rho(300\,\text{K})/\rho_o$] of about 18.4 for our single-crystalline $Sr_3Ir_4Sn_{13}$.

It is instructive to mention that the electron-electron scattering rate at low temperatures should grow as T^2 in the Fermi liquid picture. The Kadowaki-Woods ratio A/γ^2 is usually used to determine the strength of the electronic correlation of the studied system [19]. Taking $A = 0.009$ $\mu\Omega$ cm/K^2 and the low-temperature specific heat coefficient $\gamma = 39.3$ mJ/mol K^2 obtained by Kase *et al.* [1], we found $A/\gamma^2 = 0.58 \times 10^{-5}$ $\mu\Omega$ cm/(mJ/mol K^2)^2 for $Sr_3Ir_4Sn_{13}$. Enhancement of γ can be due to electron-phonon and electron-electron effects. Based on the reported electron-phonon coupling constant $\lambda_{ep} = 0.983$ and the recent band-structure calculated Fermi-level density of states (DOS) of approximately 12.5 states/eV f.u. [1,20], we deduced the electron-electron enhancement term to be $\lambda_{ee} = 24.8$, leading to the electronic specific heat coefficient $\gamma_e = 37.8$ mJ/mol K^2. Thus, it is more realistic to use γ_e for calculating the Kadowaki-Woods ratio, yielding the ratio of $A/\gamma_e^2 = 0.63 \times 10^{-5}$ $\mu\Omega$

cm/(mJ/mol K^2)^2 for $Sr_3Ir_4Sn_{13}$. This value is found to be comparable to those of heavy fermion systems [21], indicating the importance of the strongly correlated effect on the low-temperature state of $Sr_3Ir_4Sn_{13}$. Here, we also demonstrated that the large γ value is mainly enhanced by the electron-electron effect.

It is worthwhile comparing these results to those of $Ca_3Ir_4Sn_{13}$ which exhibits superconducting behavior below $T_c = 7$ K and anomalous features at $T^* = 38$ K [22–26]. Yang *et al.* estimated $A/\gamma_e^2 = 1.14 \times 10^{-5}$ $\mu\Omega$ cm/(mJ/mol K^2)^2 for $Ca_3Ir_4Sn_{13}$ [22], very close to the value originally identified as characteristic of heavy fermion materials [27]. It is interesting that the band-structure-calculated Fermi-level DOS of 12.5 states/eV f.u. and the extracted low-temperature specific heat coefficient $\gamma = 39$–41 mJ/mol K^2 for $Ca_3Ir_4Sn_{13}$ are almost the same as those of $Sr_3Ir_4Sn_{13}$ [20,22,24]. Therefore, this comparison provides evidence for the strong electron-electron correlation on the low-temperature state of $Ca_3Ir_4Sn_{13}$, similar to the present case of $Sr_3Ir_4Sn_{13}$.

B. Hall coefficient

For the Hall coefficient measurement, the single-crystal slabs with a flat surface of crystalline (110) plane were cut into dimensions of $2.5 \times 0.8 \times 0.08$ mm^3. Five leads were soldered with indium and a Hall-measurement geometry was constructed to allow simultaneous measurements of both longitudinal (ρ_{xx}) and transverse (Hall) resistivities (ρ_{xy}) using standard dc techniques. The contact size was miniaturized as small as possible (<0.2 mm) to avoid large inaccuracy in the determination of resistivities. Hall voltages were taken in opposing fields up to 6 T and with an in-plane current density of about 60 A/cm^2.

Figure 2(a) shows the temperature variation of the Hall coefficient R_H for $Sr_3Ir_4Sn_{13}$ measured at a constant field $H = 3$ T. The negative sign in R_H at temperatures above 150 K indicates that the electron-type carriers dominate its electrical transport. Upon further cooling, a sharp change in R_H accompanying with a sign change takes place below T^*. The strong temperature dependence of R_H suggests a multiband character of the Fermi surfaces. Here a simple two-band picture is sufficient for the realization of the Fermi surface structure as

$$R_H = \frac{\sigma_n^2 R_n + \sigma_p^2 R_p}{(\sigma_n + \sigma_p)^2}, \tag{2}$$

where $R_{n,p}$ and $\sigma_{n,p}$ represent the Hall coefficients and electrical conductivities for the n- and p-type carriers from electronic and hole bands, respectively. In principle, each parameter is governed by the scattering relaxation time which varies differently with temperature. At low temperatures, the p-type carriers have a dominant contribution, leading to a positive sign in R_H. A noticeable downturn in R_H appears below 25 K, implying that multiscattering channels are involved. A similar peak feature prior to T_c has been reported in the strong coupling superconductor of $SrPt_3P$ [28], suggesting that the joined scattering mechanism plays an important role for the unconventional superconductivity in this material. Such a scenario could be appropriate to the present case of $Sr_3Ir_4Sn_{13}$.
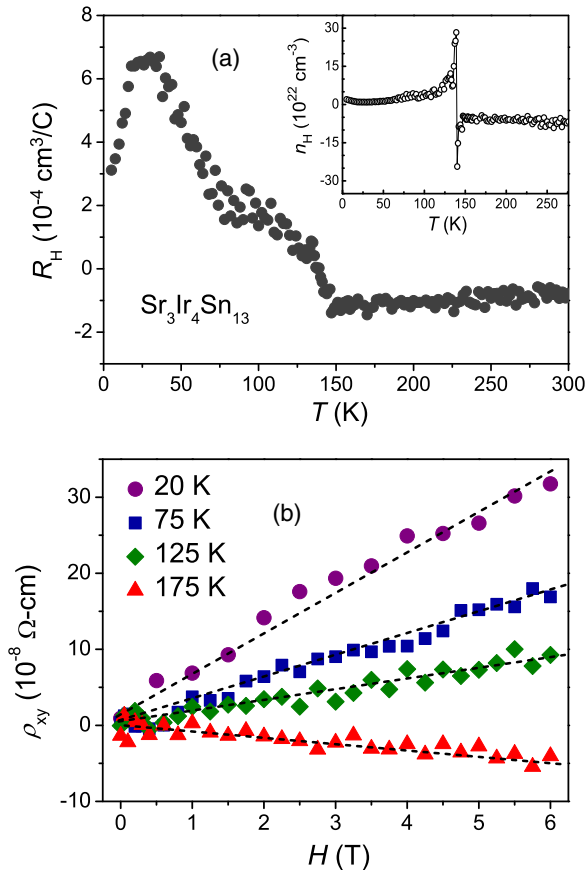
FIG. 3. (Color online) Temperature dependence of the Seebeck coefficient S for $Sr_3Ir_4Sn_{13}$. The arrow indicates the position of T^*.

experimental techniques for these measurements can be found elsewhere [29]. It is known that the Seebeck coefficient is a sensitive probe for the phenomenon associated with changes in the Fermi surfaces, such as CDW ordering and crystallographic distortion [6,30]. The plot of the measured Seebeck coefficient as a function of temperature for $Sr_3Ir_4Sn_{13}$ is given in Fig. 3. As one can see, the strong temperature variation of S gives evidence for the presence of a multiband effect. We thus employed a two-band model as in the case for the Hall coefficient analysis as

$$S = \frac{\sigma_n S_n + \sigma_p S_p}{\sigma_n + \sigma_p},$$

where $S_{n,p}$ are the Seebeck coefficients for the n- and p-type carriers, respectively. For $T < T^*$, the positive sign of S signifies that the hole-type carriers dominate the thermo-electric transport, being consistent with the observation from the Hall measurement. With raising temperature above T^*, a drastic change in the feature of S has been noticed. This phenomenon can be understood by an increasing contribution from the n-type carriers, indicating substantial modification in the Fermi surfaces across the phase transition. It is worthwhile mentioning that the present S feature is quite similar to that of $SmNiC_2$ [16], which has been identified as a 3D CDW system [13–18]. The comparison thus suggests the possible CDW ordering associated with the observed phase transition in $Sr_3Ir_4Sn_{13}$.

D. Thermal conductivity

Figure 4 illustrates the temperature dependence of the observed thermal conductivity κ for $Sr_3Ir_4Sn_{13}$. In the vicinity of T^*, a clear drop in κ, indicated by an arrow, was observed. In principle, the total thermal conductivity for an ordinary metal is a sum of electronic and lattice terms. The electronic thermal conductivity (κ_e) can be evaluated using the Wiedemann-Franz law $\kappa_e \rho / T = L_o$, where ρ is the experimental dc electric resistivity and $L_o = 2.45 \times 10^{-8}$ WΩ K^{-2} is the theoretical Lorenz number. The extracted T-dependent κ_e for $Sr_3Ir_4Sn_{13}$ above 50 K is displayed in Fig. 4. Remarkably, κ_e also exhibits a kink at around T^*, and the feature is identical to the observed κ. This analysis thus provides a confirmation that the drop in κ

FIG. 2. (Color online) (a) Hall resistivity as a function of temperature for $Sr_3Ir_4Sn_{13}$ measured at $H = 3$ T. The inset shows the temperature dependence of the Hall carrier concentration. (b) Magnetic field dependence of the Hall resistivity ρ_{xy} at various temperatures. Each dashed straight line represents linear behavior.

We also carried out the magnetic field dependence of the transverse Hall resistivity ρ_{xy} for $Sr_3Ir_4Sn_{13}$ below and above T^*. As displayed in Fig. 2(b), the plot of the ρ_{xy}-H curve shows conventional linear behavior for each temperature, confirming the absence of anomalous Hall effects in the present experiment. The inset of Fig. 2(a) illustrates the temperature dependence of the Hall carrier concentration n_H, obtained from $1/(R_H e)$. The magnitude of n_H was estimated to be about 10^{23} cm^{-3} at room temperature, indicative of the high carrier density for $Sr_3Ir_4Sn_{13}$. The prominent change in both sign and magnitude of n_H appears near T^*, providing strong evidence for a significant change of the electronic band structure across the phase transition. Therefore, the reduction in n_H could be realized as Fermi surface nesting associated with the superlattice distortion. The abrupt decrease in the carrier density below T^* has also been found in the isostructural compound of $Ca_3Ir_4Sn_{13}$, suggesting a similar phase transition mechanism for both systems [24].

C. Seebeck coefficient

Seebeck coefficient and thermal conductivity experiments were simultaneously performed in a closed cycle refrigerator using a heat pulse technique. Further details about the
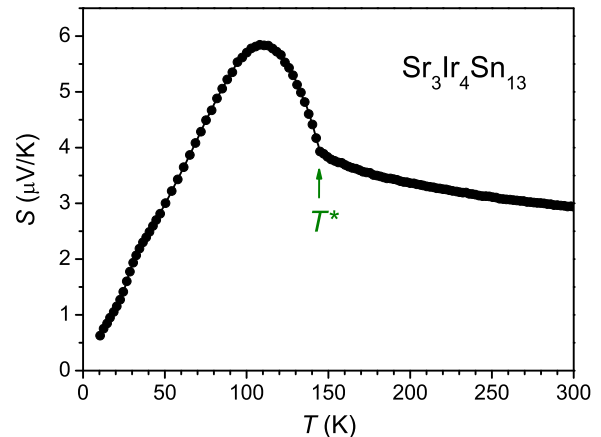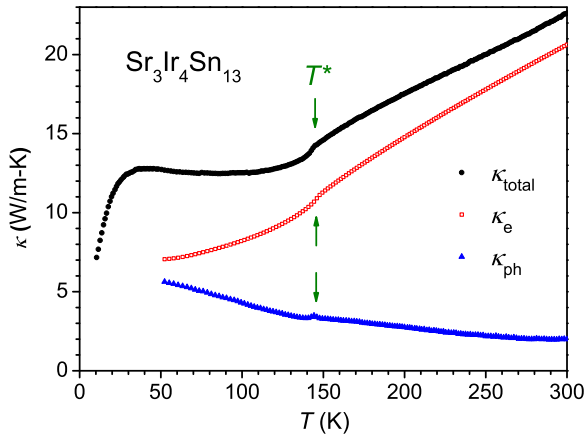
FIG. 4. (Color online) Temperature variation of the total thermal conductivity κ for $Sr_3Ir_4Sn_{13}$. The electronic thermal conductivity κ_e was evaluated using the Wiedemann-Franz law. The lattice thermal conductivity κ_L was obtained by subtracting κ_e from the experimental κ. The arrows highlight the position of T^*.

FIG. 5. (Color online) Temperature variation of the specific heat C_P for $Sr_3Ir_4Sn_{13}$. The absence of thermal hysteresis near T^* indicates the second-order nature of this phase transition. The dashed curve represents the background estimated by fitting the lattice specific heat through the experimental data far from the transition region. Inset: A $\Delta C_p/T$ vs T plot in the vicinity of T^*.

near T^* is essentially caused by the reduction of the electronic contribution.

The lattice thermal conductivity (κ_L), obtained by subtracting κ_e from the experimental κ, is presented in Fig. 4. It is clear that a small peak in κ_L is discerned in the vicinity of T^*. Similar observations have been reported in the CDW superconductors of $Lu_5Ir_4Si_{10}$ and $Lu_5Rh_4Si_{10}$ [6,31]. The excess κ_L has been attributed to the considerable heat carried by the soft phonons during the phase transition. Such a scenario could be appropriate for the present case of $Sr_3Ir_4Sn_{13}$. As a matter of fact, the calculated phonon dispersion indicated several soft phonon modes are responsible for the structural distortion associated with T^* of $Sr_3Ir_4Sn_{13}$ [20].

E. Specific heat

Specific heat measurement was performed with a high-resolution ac calorimeter, using chopped light as a heat source. Further details about the experimental techniques for these measurements can be found elsewhere [6]. The temperature-dependent specific heat of $Sr_3Ir_4Sn_{13}$ is shown in Fig. 5. A spiky feature in C_p demonstrates the appearance of a sharp phase transition at $T^* = 147$ K. The absence of thermal hysteresis indicates that this transition is second order or weak first order in nature. To evaluate the change of the entropy associated with the phase transition, we first determined the specific heat jump $\Delta C_p \simeq 20.2$ J/mol K by subtracting a smooth background, estimated by fitting the lattice specific heat through the experimental data far from the transition region. This also reveals an excess specific heat $\Delta C_p/C_p \simeq 14\%$ at T^*. The temperature dependence of $\Delta C_p/T$ around the phase transition is shown in the inset of Fig. 5. A large entropy change of $\Delta S \simeq 0.17R$ (where R is the ideal gas constant) was obtained by integrating $\Delta C_p/T$ through the entire transition region.

It is worthwhile comparing these results to those of $Lu_5Ir_4Si_{10}$, which also exhibits a huge specific heat jump near its CDW phase transition temperature of about 83 K. The values of $\Delta C_p \simeq 55$ and $\simeq 160$ J/mol K have been reported
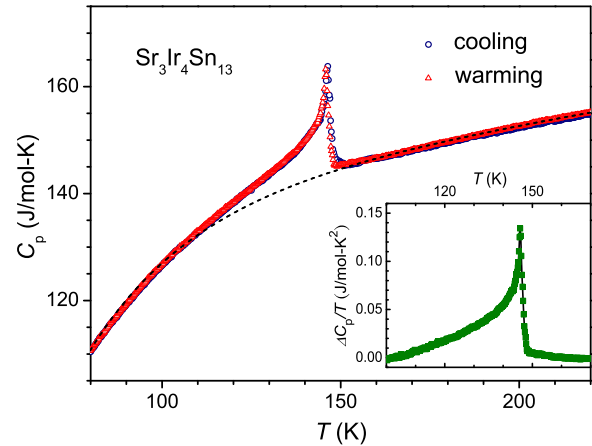
for the polycrystalline and single-crystalline $Lu_5Ir_4Si_{10}$ [5,6]. The corresponding large entropy changes $\Delta S \simeq 0.17R$ and $\simeq 0.5R$ lead to the conclusion that the nature of CDW in $Lu_5Ir_4Si_{10}$ is beyond the mean-field description. Since the CDW in $Lu_5Ir_4Si_{10}$ is associated with the lattice distortion within its 3D crystal structure, it seems that the appearance of a large specific heat anomaly is a common feature among the CDW materials arising from lattice instability. Therefore, the exhibited C_p behaviors in $Sr_3Ir_4Sn_{13}$ are reminiscent of those observed in $Lu_5Ir_4Si_{10}$, indicative of a similar origin for both phase transitions.

F. Nuclear magnetic resonance

Nuclear magnetic resonance is known as a site-selective tool, yielding the local information of structural and electronic characteristics for the studied material. In this investigation, NMR measurements were carried out using a Varian 300 spectrometer, with a constant field of 7.0868 T. A home-built probe was employed for both room-temperature and low-temperature experiments [32,33]. To avoid the skin depth problem of the rf transmission power, we used a powder sample by crushing the single crystals of $Sr_3Ir_4Sn_{13}$. The specimen was put in a plastic vial that showed no observable ^{119}Sn NMR signal.

^{119}Sn (nuclear spin $I = 1/2$) NMR spectra which were mapped out by integrating spin echo signals of various excitations are displayed in Fig. 6. Two ^{119}Sn NMR resonance lines have been resolved at room temperature. Such an observation is consistent with the existence of two nonequivalent crystallographic Sn sites, denoted as Sn1 and Sn2, in the cubic $Pm\bar{3}n$ phase. We assigned the high-frequency line to Sn1 since the Sn1 atoms occupy the axially symmetric 2a site (in Wyckoff notations). On the other hand, the Sn2 atoms reside at the 24k site, which is nonaxially symmetric, and the recognizable NMR line shape exhibits two distinctive shoulders due to anisotropic Knight shift effects. The simulated line shapes for
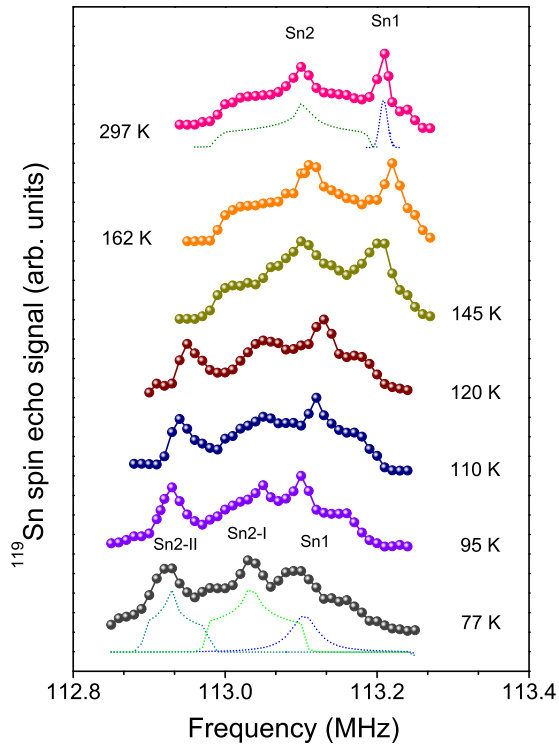
FIG. 6. (Color online) Evolution of ^{119}Sn NMR spectrum of $Sr_3Ir_4Sn_{13}$ measured at various temperatures. Above T^*, each spectrum shows resolved contributions from two Sn sites. The dotted curves at 297 K are simulated results for the Sn1 and Sn2 sites, respectively. Distinctive Sn2-I and Sn2-II NMR resonance lines appear in the spectra at low temperatures. The simulated curves at 77 K represent isolated components for the Sn1, Sn2-I, and Sn2-II sites, respectively.

both Sn1 and Sn2 sites were plotted as dotted curves beneath the data points taken at 297 K. Note that the line-shape areas for Sn1 and Sn2 agree with a ratio of 1:12, according to their site occupations within the $Yb_3Rh_4Sn_{13}$-type structure.

To gain more insight into the evolution of the line shape across the phase transition, we provide several representative spectra taken below and above T^*. It is apparent that the linewidth does not exhibit a dramatic broadening at low temperatures, signifying the nonmagnetic origin for this phase transition. Below T^*, the Sn2 site splits into two peaks, labeled as Sn2-I and Sn2-II, respectively, indicating the occurrence of two different Sn2 atomic environments. The observed line shape can be reproduced from simulation, shown as dotted curves beneath the data points at 77 K. However, the number of the observed peaks is less than that of the nonequivalent crystallographic Sn sites revealed from the analysis of low-T XRD [2]. Accordingly, there are four nonequivalent Sn2 sites due to the distortion of the Sn2 icosahedra within the $Pm\bar{3}n$ phase. It is not clear why these values differ, but it is possible for these to be reconciled if the corresponding spin susceptibility among some Sn sites is similar, leading to partially unresolved NMR line separation as observed. Alternatively, the additional Sn2 NMR line below T^* could be a consequence of the CDW formation. In the commensurate CDW phase, the appearance of one or more NMR splitting lines is expected because of the influence of the periodic
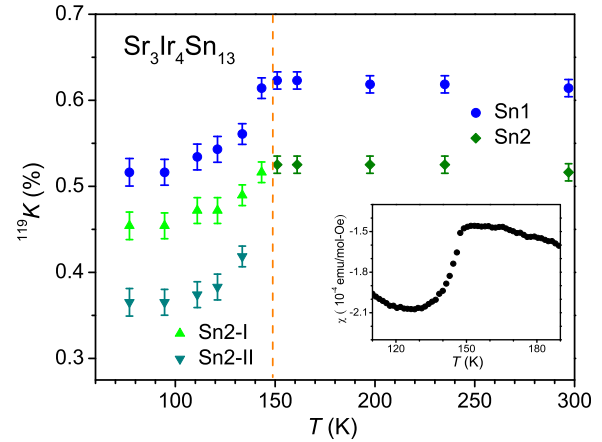

FIG. 7. (Color online) Temperature-dependent ^{119}Sn NMR Knight shifts for $Sr_3Ir_4Sn_{13}$. The dashed vertical line indicates the phase transition temperature. The inset shows the magnetic susceptibility χ of $Sr_3Ir_4Sn_{13}$ in the vicinity of T^*.

modulation in the electronic density on the probed nuclei [34]. Such line splitting behavior has been observed in the well-established commensurate CDW phase of $2H$-$TaSe_2$ below 90 K [35–37].

Figure 7 illustrates the temperature dependence of the ^{119}Sn NMR Knight shift ^{119}K for each Sn site of $Sr_3Ir_4Sn_{13}$, obtained from the simulated result of the individual NMR spectrum. The values of ^{119}K were referred to the ^{119}Sn resonance frequency $\nu_R = 112.519$ MHz, evaluated from the nuclear gyromagnetic ratio $^{119}\gamma_N/2\pi = 1.5867$ MHz/kOe. The Knight shift here is a sum of three parts as $^{119}K = K_{orb} + K_s + K_{sd}$. The first term K_{orb} is the orbital shift due to the contribution from the Van Vleck orbital magnetism and the second one K_s arises from Sn s character electrons. The effect arising from p electrons can be neglected, due to relatively weak core polarization from p orbitals [38]. The third term K_{sd} reflects the Ir $5d$ electronic behavior through the transferred hyperfine interaction via conduction electrons. As one can see, the Knight shifts are almost temperature independent for both Sn1 and Sn2 sites as $T > T^*$, in good agreement with the characteristic of a paramagnet. Lowering the temperature below T^*, each Knight shift changes progressively with a rapid drop, consistent with the feature found in the bulk magnetic susceptibility χ shown in the inset of Fig. 7. Therefore, the NMR Knight shift analysis provides microscopic evidence that the reduction in χ is partially related to the decrease in the Sn $5s$ and Ir $5d$ electronic states of $Sr_3Ir_4Sn_{13}$. With this accordance, it indicates that the interplay between electronic and structural instability is responsible for the peculiar phase transition in $Sr_3Ir_4Sn_{13}$.

III. CONCLUSIONS

The present investigation shows clear evidence for a pronounced phase transition in the vicinity of $T^* = 147$ K in $Sr_3Ir_4Sn_{13}$. Based on the analyses of the anomalous signatures in the temperature dependencies of ρ, R_H, S, and κ_e near T^*, we obtained a precise picture that the characteristics of the phase transition are highly associated with the electronic state reconstruction at Fermi surfaces. In addition, the NMR observations provide concrete evidence that the Fermi surface

modification is essentially related to the slight displacement and/or distortion of the Sn2 atom from its initial position within the $Yb_3 Rh_4 Sn_{13}$-type structure. While the observed phase transition behavior in $Sr_3Ir_4Sn_{13}$ resembles the CDW formation in many aspects, the unambiguous CDW state in $Sr_3Ir_4Sn_{13}$ will have to wait until there is identification of charge modulation along a specific wave vector direction by means of a high-resolution transmission electron microscopy (HRTEM) [12,39].

[1] N. Kase, H. Hayamizu, and J. Akimitsu, Phys. Rev. B **83**, 184509 (2011).

[2] L. E. Klintberg, S. K. Goh, P. L. Alireza, P. J. Saines, D. A. Tompsett, P. W. Logg, J. Yang, B. Chen, K. Yoshimura, and F. M. Grosche, Phys. Rev. Lett. **109**, 237008 (2012).

[3] R. N. Shelton, L. S. Hausermann-Berg, P. Klavins, H. D. Yang, M. S. Anderson, and C. A. Swenson, Phys. Rev. B **34**, 4590 (1986).

[4] H. D. Yang, P. Klavins, and R. N. Shelton, Phys. Rev. B **43**, 7681 (1991).

[5] B. Becker, N. G. Patil, S. Ramakrishnan, A. A. Menovsky, G. J. Nieuwenhuys, J. A. Mydosh, M. Kohgi, and K. Iwasa, Phys. Rev. B **59**, 7266 (1999).

[6] Y.-K. Kuo, C. S. Lue, F. H. Hsu, H. H. Li, and H. D. Yang, Phys. Rev. B **64**, 125124 (2001).

[7] Y. -K. Kuo, F. H. Hsu, H. H. Li, H. L. Huang, C. W. Huang, C. S. Lue, and H. D. Yang, Phys. Rev. B **67**, 195101 (2003).

[8] S. van Smaalen, M. Shaz, L. Palatinus, P. Daniels, F. Galli, G. J. Nieuwenhuys, and J. A. Mydosh, Phys. Rev. B **69**, 014103 (2004).

[9] M. Inamdar and S. Ramakrishnan, Phys. Rev. B **77**, 113103 (2008).

[10] R. Tediosi, F. Carbone, A. B. Kuzmenko, J. Teyssier, D. van der Marel, and J. A. Mydosh, Phys. Rev. B **80**, 035107 (2009).

[11] F. Galli, S. Ramakrishnan, T. Taniguchi, G. J. Nieuwenhuys, J. A. Mydosh, S. Geupel, J. Ludecke, and S. van Smaalen, Phys. Rev. Lett. **85**, 158 (2000).

[12] C. M. Tseng, C. H. Chen, and H. D. Yang, Phys. Rev. B **77**, 155131 (2008).

[13] S. Shimomura, C. Hayashi, G. Asaka, N. Wakabayashi, M. Mizumaki, and H. Onodera, Phys. Rev. Lett. **102**, 076404 (2009).

[14] J. Laverock, T. D. Haynes, C. Utfeld, and S. B. Dugdale, Phys. Rev. B **80**, 125111 (2009).

[15] A. Wolfel, L. Li, S. Shimomura, H. Onodera, and S. van Smaalen, Phys. Rev. B **82**, 054120 (2010).

[16] J. H. Kim, J. S. Rhyee, and Y. S. Kwon, Phys. Rev. B **86**, 235101 (2012).

[17] N. Hanasaki, Y. Nogami, M. Kakinuma, S. Shimomura, M. Kosaka, and H. Onodera, Phys. Rev. B **85**, 092402 (2012).

[18] B. Woo, S. Seo, E. Park, J. H. Kim, D. Jang, T. Park, H. Lee, F. Ronning, J. D. Thompson, V. A. Sidorov, and Y. S. Kwon, Phys. Rev. B **87**, 125121 (2013).

[19] K. Kadowaki and S. B. Woods, Solid State Commun. **58**, 507 (1986).

[20] D. A. Tompsett, Phys. Rev. B **89**, 075117 (2014).

[21] N. Tsujii, H. Kontani, and K. Yoshimura, Phys. Rev. Lett. **94**, 057201 (2005).

[22] J. Yang, B. Chen, C. Michioka, and K. Yoshimura, J. Phys. Soc. Jpn. **79**, 113705 (2010).

[23] H. Hayamizu, N. Kase, and J. Akimitsu, Physica C **470**, S541 (2010).

[24] K. Wang and C. Petrovic, Phys. Rev. B **86**, 024522 (2012).

[25] S. Y. Zhou, H. Zhang, X. C. Hong, B. Y. Pan, X. Qiu, W. N. Dong, X. L. Li, and S. Y. Li, Phys. Rev. B **86**, 064504 (2012).

[26] S. Gerber, J. L. Gavilano, M. Medarde, V. Pomjakushin, C. Baines, E. Pomjakushina, K. Conder, and M. Kenzelmann, Phys. Rev. B **88**, 104505 (2013).

[27] G. R. Stewart, Rev. Mod. Phys. **56**, 755 (1984).

[28] T. Takayama, K. Kuwano, D. Hirai, Y. Katsura, A. Yamamoto, and H. Takagi, Phys. Rev. Lett. **108**, 237001 (2012).

[29] C. S. Lue, S. H. Yang, A. Abhyankar, Y. D. Hsu, H. T. Hong, and Y. K. Kuo, Phys. Rev. B **82**, 045111 (2010).

[30] Y. K. Kuo, K. M. Sivakumar, T. H. Su, and C. S. Lue, Phys. Rev. B **74**, 045115 (2006).

[31] C. S. Lue, Y.-K. Kuo, F. H. Hsu, H. H. Li, H. D. Yang, P. S. Fodor, and L. E. Wenger, Phys. Rev. B **66**, 033101 (2002).

[32] C. S. Lue, H. F. Liu, S. L. Hsu, M. W. Chu, H. Y. Liao, and Y. K. Kuo, Phys. Rev. B **85**, 205120 (2012).

[33] H. F. Liu, C. N. Kuo, C. S. Lue, K.-Z. Syu, and Y. K. Kuo, Phys. Rev. B **88**, 115113 (2013).

[34] P. -J. Chu, B. C. Gerstein, H. D. Yang, and R. N. Shelton, Phys. Rev. B **37**, 1796 (1988).

[35] F. Borsa, D. R. Torgeson, and H. R. Shanks, Phys. Rev. B **15**, 4576 (1977).

[36] B. H. Suits, S. Couturie, and C. P. Slichter, Phys. Rev. Lett. **45**, 194 (1980).

[37] L. Pfeiffer, R. E. Walstedt, R. F. Bell, and T. Kovacs, Phys. Rev. Lett. **49**, 1162 (1982).

[38] *Metallic Shifts in NMR*, edited by G. C. Carter, L. H. Bennett, and D. J. Kahan (Pergamon, Oxford, 1977).

[39] M. H. Lee, C. H. Chen, M.-W. Chu, C. S. Lue, and Y. K. Kuo, Phys. Rev. B **83**, 155121 (2011).